PAPER • OPEN ACCESS

Emergent magnonic singularities in anti parity-time symmetric synthetic antiferromagnets

To cite this article: Chao-Wei Sui *et al* 2022 *New J. Phys.* **24** 023031

New Journal of Physics
The open access journal at the forefront of physics

Deutsche Physikalische Gesellschaft DPG
IOP Institute of Physics

Published in partnership with: Deutsche Physikalische Gesellschaft and the Institute of Physics

OPEN ACCESS

RECEIVED
8 December 2021

REVISED
29 January 2022

ACCEPTED FOR PUBLICATION
8 February 2022

PUBLISHED
24 February 2022

PAPER

Emergent magnonic singularities in anti parity-time symmetric synthetic antiferromagnets

Chao-Wei Sui[1], **Shao-Hua Yuan**[1], **Xi-Guang Wang**[2], **Jamal Berakdar**[3,*] and **Chenglong Jia**[1,4,*]

[1] Key Laboratory for Magnetism and Magnetic Materials of the Ministry of Education, Lanzhou University, Lanzhou 730000, People's Republic of China
[2] School of Physics and Electronics, Central South University, Changsha 410083, People's Republic of China
[3] Institut für Physik, Martin-Luther Universität Halle-Wittenberg, D-06120 Halle/Saale, Germany
[4] Lanzhou Center for Theoretical Physics & Key Laboratory of Theoretical Physics of Gansu Province, Lanzhou University, Lanzhou 730000, People's Republic of China
[*] Authors to whom any correspondence should be addressed.

E-mail: Jamal.Berakdar@physik.uni-halle.de and cljia@lzu.edu.cn

Keywords: spin waves, synthetic antiferromagnet, parity-time symmetry, spontaneous symmetry breaking, magnonic singularities

Abstract

We study the impact of the transition across the anti-parity-time (anti-$\mathcal{PT}$) symmetry breaking point on the low-energy spin excitations in a synthetic antiferromagnet (SyAFM) that consists of two magnetic layers coupled antiferromagnetically via the Ruderman–Kittel–Kasuya–Yosida (RKKY) interaction. When varying the interlayer (RKKY) coupling strength a degeneracy point (exceptional point) is reached beyond which the system enters the anti-$\mathcal{PT}$ symmetry-broken phase. This phase is marked by the emergence of a finite net magnetization and low-lying excitations beyond the *Goldstone modes* in the anti-$\mathcal{PT}$ symmetry-preserved phase. For systems hosting an interfacial Dzyaloshinskii–Moriya interaction, we find a bound state in the continuum with a maximal coherent superposition of SyAFM excitations without any radiation. Analytical results for linearized models are corroborated with full numerical micromagnetic simulations endorsing the robustness and generalities of the theory predictions.

1. Introduction

Antiferromagnetic (AFM) materials with zero net magnetization offer an exciting platform for information handling that is robust against magnetic field perturbations and magnetic crosstalk between neighboring devices [1]. Here, we focus on synthetic antiferromagnetic (SyAFM) structures which are fabricated out of two ferromagnetic (FM) layers and are coupled via Ruderman–Kittel–Kasuya–Yosid (RKKY) interaction. SyAFMs allow for electrical manipulation of AFM ordering and are convenient to investigate using well-developed techniques for ferromagnets [2]. Recent research on their collective excitations, the spin waves (with magnons as quanta of excitations) [3–7], demonstrated their potential for logic gates, information processing, and sensory devices with low power operation [8–10]. Unlike FM systems with only right-handed spin wave modes, AFMs have two degenerate spin wave eigenmodes with opposite circular polarization, referred to as right- and left-handed magnons depending on the precessional handiness of the Néel vector [3, 11, 12] (cf figure 1). Any polarization state can be produced by a combination of these two eigenmodes, providing a way to encode information based on the spin wave polarization as well as on the amplitude and phase. Adverse however is that, the two-fold degeneracy is protected by the combined symmetry of time-reversal and sub-lattice exchange, and we have thus to seek controlled interactions that break either or both of the two symmetries. A way to achieve that is presented in this study.

The magnetic dynamic is generically non-unitary due to the ubiquitous magnetic damping. Hence, the Hamiltonian governing the low energy (spin wave) modes can be intrinsically non-Hermitian, and may

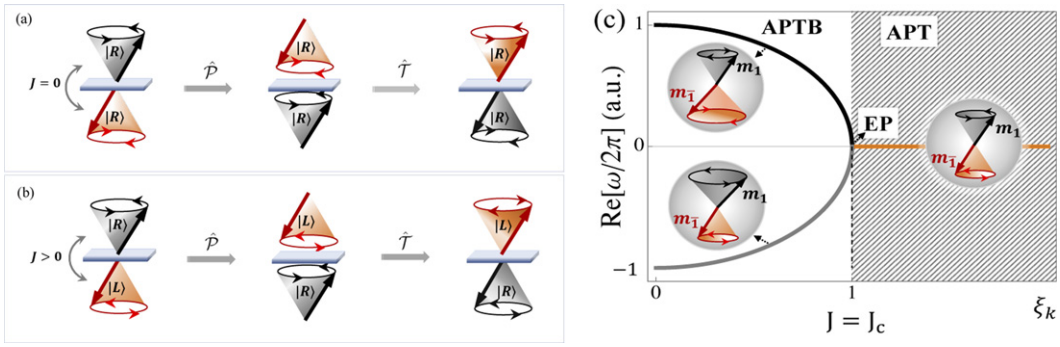

Figure 1. $\mathcal{PT}$ symmetric property of SyAFM structures. Red and black arrows represent the layers two antiparallel magnetic moments $\vec{m}_1$ and $\vec{m}_{\bar{1}}$ with the layers normal $\hat{e}_z$ being along the easy axis. $|\mathrm{R}\rangle$ and $|\mathrm{L}\rangle$ denote the locally right- and left-handed precessions around the equilibrium easy-direction of $\langle\vec{m}_n\rangle$. The vectors $\vec{m}_1$ and $\vec{m}_{\bar{1}}$ are exchanged under the parity operation $\hat{\mathcal{P}}$. The time-reversal operation $\hat{\mathcal{T}}$ leads to $\vec{m}_n \to -\vec{m}_n$, while the handiness ($|\mathrm{R}\rangle$ or $|\mathrm{L}\rangle$) of the local precessional remains unchanged under the time reversal $\hat{\mathcal{T}}$. (a) If the interlayer interaction strength vanishes ($J = 0$), the magnetization dynamics in each layer is characterized by right-handed modes which are shown to be eigenstates of $\hat{\mathcal{P}}\hat{\mathcal{T}}$; (b) as $J > J_c$, the precessions of neighboring magnetic moments $\vec{m}_1$ and $\vec{m}_{\bar{1}}$ are bundled anti-parallel around the Néel vector and the modes are shown to be eigenstates of the anti-$\mathcal{PT}$ (APT) operation. (c) The real parts of the magnonic eigenmode energies as a function of the scaled interlayer interaction strength J. Shown are the anti-$\mathcal{PT}$ symmetric SyAFM phase $J > J_c$, and the region below the exceptional point (EP with $J = J_c$) corresponding to the APT broken (APTB) phase ($J < J_c$). Note, the slightly different ratios between the cone angles of $\vec{m}_1$ and $\vec{m}_{\bar{1}}$ in leading to the emergence of a finite magnetization.

become defective at special conditions (exceptional points, EPs) depending on the external parameters. At these (degeneracy) points the number of eigenvalues (algebraic multiplicity) exceeds the number of eigenvectors (geometric multiplicity). For FM structure, various facets of how EPs affect the magnetic dynamics were discussed. We are concerned with SyAFMs. Such (interacting) systems are suitable for studying anti-parity-time (anti-$\mathcal{PT}$) symmetry behavior (in contrast, FM structures with balanced gain and loss magnetic damping are related to $\mathcal{PT}$ symmetry [13–30]). Different interlayer coupling (RKKY) strengths J correspond to different free-energy densities of the SyAFMs. At a certain value of the interaction strength $J = J_c$ a degeneracy (or EP) in the relevant low-energy modes occur and the modes undergo a symmetry change: for $J < J_c$ the anti-$\mathcal{PT}$ symmetry is broken (APTB phase), while for $J > J_c$ the anti-$\mathcal{PT}$ symmetry (APT) is preserved. The degree of degeneracy is related to the order of the EP, which in turn can be tuned by structural design [31]. The value of J_c depends on other determining parameters of the free energy density such as the magnetic anisotropy and exchange energy as well as on magnetic damping and is given explicitly in the next section. In the APT phase the system has an imaginary spectrum. In the APTB phase the spectrum is complex [32–40].

The anti-$\mathcal{PT}$ phase transition point J_c can be reached by scanning J or the other parameters in the free energy density. Experimentally, electric tuning of J were realized in SyAFM structures, e.g. FeCoB/Ru/FeCoB and $(\mathrm{Pt/Co})_2$/Ru/$(\mathrm{Pt/Co})_2$ [41, 42], in which not only the amplitude but also the sign of RKKY interaction can be tuned by changing gate voltages. Thus, when we discuss below properties with varying J we implicitly mean that there is some external fields (such as gate voltage) which are varied affecting the respective changes in J (and hence the free energy density). Furthermore, the magneto-electric interactions upon interfacing an FM layer with a ferroelectrics allows for an electrical control of the magnetization damping [43–45] and the magnetic anisotropy [46, 47].

Considering SyAFMs with an interfacial Dzyaloshinskii–Moriya interaction (DMI), we find that a magnonic bound state in the continuum (BIC) is formed. This hybrid BIC cannot radiate away and consists of a maximally coherent superposition of modes of the two FM layer. The above statement are inferred analytically from a linearized model and confirmed with full numerical micromagnetic simulations.

2. Results

Anti-$\mathcal{PT}$ symmetric SyAFM dynamics. The magnetic dynamics in a SyAFM is describable by coupled Landau–Lifshitz–Gilbert (LLG) equations [48]. For two coupled layers we write

$$\partial_t m_n = -\frac{\gamma_n}{1+\alpha_n^2}\mathbf{m}_n \times \left[\mathbf{H}_n^{\mathrm{eff}} + \alpha_n(\mathbf{m}_n \times \mathbf{H}_n^{\mathrm{eff}})\right]. \tag{1}$$

Here $\mathbf{m}_n$ (with $n = 1, \bar{1}$) denote the magnetization direction for two FM sublayers, γ_n is the gyromagnetic ratio, and α_n is the Gilbert damping constant. The effective magnetic field acting locally on $\mathbf{m}_n$ reads

$$\mathbf{H}_n^{\text{eff}} = 2(A_n\nabla^2\mathbf{m}_n + K_z m_n^z \hat{e}_z - J\mathbf{m}_{\bar{n}}),$$

where A_n is the Heisenberg exchange coupling constant within each m_n-layers, K_z is a magnetic anisotropy along the easy z-axis, and J is the RKKY interaction between the two sublayers.

When $J = 0$, the two layers are decoupled; each magnetization $\mathbf{m}_n$ prefers locally right-handed precessions around its own easy-direction, as sketched in figure 1(a).

A positive RKKY interaction ($J > 0$) tends to align the layers magnetization antiparallel, enforcing $\mathbf{m}_1$ and $\mathbf{m}_{\bar{1}}$ to process in the same global manner, i.e. right- or left-handed precessions around the Néel vector $\mathbf{n} = (\mathbf{m}_1 - \mathbf{m}_{\bar{1}})/2$ (cf figure 1(b)). To show that the low-energy magnetic dynamics is anti-$\mathcal{PT}$ symmetric, we linearize the LLG equations by writing $\mathbf{m}_n = m_n^0\hat{\mathbf{e}}_z + \delta\mathbf{m}_n$ with $m_n^0 \approx \pm 1$ and $|\delta\mathbf{m}_n| \ll 1$ and obtain the Schrödinger-type equation for the dynamical excitations of $\delta\mathbf{m}_n$

$$\mathrm{i}\partial_t\Psi(\mathbf{r}, t) = \mathcal{H}\Psi(\mathbf{r}, t) \tag{2}$$

where $\Psi(\mathbf{r}, t) = (\delta m_1^x - \mathrm{i}\delta m_1^y, \delta m_{\bar{1}}^x - \mathrm{i}\delta m_{\bar{1}}^y)^{\mathrm{T}}$ and

$$\mathcal{H} = \begin{bmatrix} H_1(\tilde{\gamma}_1 - \mathrm{i}\tilde{\alpha}_1) & J(\tilde{\gamma}_1 - \mathrm{i}\tilde{\alpha}_1) \\ -J(\tilde{\gamma}_{\bar{1}} + \mathrm{i}\tilde{\alpha}_{\bar{1}}) & -H_{\bar{1}}(\tilde{\gamma}_{\bar{1}} + \mathrm{i}\tilde{\alpha}_{\bar{1}}) \end{bmatrix} \tag{3}$$

with renormalized $\tilde{\gamma}_n = 2\gamma_n/(1 + \alpha_n^2)$ and $\tilde{\alpha}_n = \alpha_n\tilde{\gamma}_n$. For $J = 0$, the magnetization dynamics of uncoupled layers are governed by their own Hamiltonian $H_n = -A_n\nabla^2 + K_z + J$.

For SyAFMs with $A_1 = A_{\bar{1}} = A$, $\gamma_1 = \gamma_{\bar{1}} = \gamma$, and the same damping rates $\alpha_1 = \alpha_{\bar{1}} = \alpha$, $\mathcal{H}$ reduces to

$$\mathcal{H}' = \begin{bmatrix} H_k(1 - \mathrm{i}\alpha) & J(1 - \mathrm{i}\alpha) \\ -J(1 + \mathrm{i}\alpha) & -H_k(1 + \mathrm{i}\alpha) \end{bmatrix} \tag{4}$$

where $H_k = A\mathbf{k}^2 + K_z + J$ in the long-wavelength limit of a plane-wave ansatz $\Psi \sim \mathrm{e}^{\mathrm{i}(\mathbf{k}\cdot\mathbf{r} - \omega t)}$, where $\mathbf{k}$ stands for the wave number of propagating spin waves [49].

Symmetry considerations. The eigenvalues of $\mathcal{H}'$ are

$$\omega_\pm = H_k\left(-\mathrm{i}\alpha \pm \sqrt{1 - \xi_k^2}\right), \tag{5}$$

where $\xi_k = J\sqrt{1 + \alpha^2}/H_k$.

(a) For purely imaginary $\omega_\pm$ (when $|\xi_k| > 1$) the eigenvectors read

$$\Psi_{\text{APT}}^{\pm} = \begin{bmatrix} \operatorname{sech}\varphi \pm \mathrm{i}\tanh\varphi \\ -\mathrm{e}^{\mathrm{i}\eta} \end{bmatrix}, \tag{6}$$

where $\tanh\varphi = \sqrt{1 - 1/\xi_k^2}$ and $\tan\eta = \alpha$. A parity operation $\hat{\mathcal{P}}$ corresponds to applying the Pauli operator $\sigma_x = \begin{bmatrix} 0 & 1 \\ 1 & 0 \end{bmatrix}$. The time-reversal $\hat{\mathcal{T}}$ corresponds to $i \to -i$, $t \to -t$ and $\mathbf{r} \to \mathbf{r}$. The states, given by equation (6), $\Psi_{\text{APT}}^{\pm}$ are also eigenvectors of the $\hat{\mathcal{P}}\hat{\mathcal{T}}$ operator [50], satisfying $\hat{\mathcal{P}}\hat{\mathcal{T}}\Psi_{\text{APT}}^{\pm} = \lambda_\pm\Psi_{\text{APT}}^{\pm}$ with $|\lambda_\pm|^2 = 1$. The anticommutator $\{\mathcal{H}', \hat{\mathcal{P}}\hat{\mathcal{T}}\}$ vanishes. Thus, $\mathcal{H}'$ of a coupled SyAFM possesses an anti-$\mathcal{PT}$ symmetry. This symmetry is preserved till J reaches

$$J_{\text{c}} = |H_k/\sqrt{1 + \alpha^2}|, \tag{7}$$

where the EP occurs at $J = H_k/\sqrt{1 + \alpha^2}$ (cf figure 1(c)). Physically this means, the dynamic motions of $\mathbf{m}_1$ and $\mathbf{m}_{\bar{1}}$ in the two magnetic layers are *equator modes*, sharing the same amplitude. No net dynamic magnetization is generated.

(b) For smaller $J < J_{\text{c}}$ the system enters anti-$\mathcal{PT}$ symmetry-broken (APTB) phase with complex eigenvalues ($|\xi_k| < 1$). The corresponding eigenvectors [51] are given by

$$\Psi_{\text{APTB}}^{+} = \begin{bmatrix} \cosh\dfrac{\phi}{2} \\ -\sinh\dfrac{\phi}{2}\,\mathrm{e}^{\mathrm{i}\eta} \end{bmatrix}, \qquad \Psi_{\text{APTB}}^{-} = \begin{bmatrix} -\sinh\dfrac{\phi}{2} \\ \cosh\dfrac{\phi}{2}\,\mathrm{e}^{\mathrm{i}\eta} \end{bmatrix} \tag{8}$$

where $\tanh\phi = \xi_k$. Considering $\cosh^2\frac{\phi}{2} > \sinh^2\frac{\phi}{2}$, one infers that $\mathbf{m}_1$ and $\mathbf{m}_{\bar{1}}$ precesses with different cone angles in two FM sublayers. The left- and right-circularity polarized modes $\Psi^{\pm}_{\rm APTB}$ around the Néel vector $\mathbf{n}$ are dominated by the precession in the upper and lower sublayers. The precessional dynamics is accompanied by the emergence of a small intrinsic magnetization $\mathbf{m} = (\mathbf{m}_1 + \mathbf{m}_{\bar{1}})/2$ whose dynamics is governed by the temporal evolution of the Néel order, $\mathbf{m} \propto (\mathbf{n} \times \partial_t \mathbf{n})$ [52]. Thus, the emergent magnetization in collinear SyAFM systems signals a breaking of anti-$\mathcal{PT}$ symmetry.

Generically, $|\xi_k| < 1$ and the anti-$\mathcal{PT}$ symmetry is broken. For isotropic SyAFMs (no magnetic anisotropy $K_z = 0$) and for a frequency at/below the ferromagnetic resonance (FMR) point $H_{k=0} = J$, no spin waves are excited, leading to $\xi_k = \sqrt{1+\alpha^2}$ and the eigenvalues $\omega_+ = 0$ and $\omega_- = -2\mathrm{i}J\alpha$. This APT phase persists in the presence of a small anisotropy, as long as $K_z/J < \alpha^2/(1+\sqrt{1+\alpha^2})$. Both eigenvalues become imaginary and their absolute values depend monotonically on K_z: $|\omega_-|$ ($|\omega_+|$) approaches increasingly (decreasingly) the Gilbert damping constant α, as K_z increases. No precessional motions are found even at FMR point in the micromagnetic simulations and $\mathbf{m}_n$ decays with time exponentially to the easy-axis.

Generally, one may argue that due to the uniaxial magnetic anisotropy, the SU(2) spin rotational symmetry is reduced to SO(2)×$\mathbb{Z}_2$. The low-lying excitations (*Goldstone modes*) are associated with the continuous SO(2) symmetry. Above the energy gap which is determined by $\mathbb{Z}_2$ symmetry, the excitation energy of the Goldstone mode should vanish when $\mathbf{k} \to \mathbf{Q}$, where $\mathbf{Q}$ is the wavevector of magnetic ordering, for example, $\mathbf{Q} = 0$ for the SyAFMs. This is indeed confirmed by figures 2(a) and (b)) (for $\alpha = 0$ or $J = 0$). However, as the Gilbert damping constant α and/or RKKY interaction J increase in a way that $\sqrt{1+\alpha^2} - 1 > K_z/J$ is satisfied, an EP emerges and the APT phase is spread out over the k-space. As a result, the real eigenfrequency of spin waves reaches its minimum value (zero) far away from the $\mathbf{Q}$-point, as shown by the results in figure 2 which follow from micromagnetic simulations using the OOMMF package. A one-dimensional SyAFM system consisting of two $1000 \times 1 \times 1$ nm^3 FM layers is considered with a mesh size of $1 \times 1 \times 1$ nm^3. The ground state equilibrium antiparallel magnetization is oriented along the z-axis. To launch the magnetization excitations, we apply the rf magnetic fields, $\tilde{h}_x(t) = h_0\,\mathrm{sinc}(\omega_c t)\hat{\mathbf{e}}_x$ with the amplitude $h_0 = 10$ mT and the cut-off frequency $\omega_c = 60$ GHz. The dispersion relation given by the fast Fourier transform (FFT) clearly indicates that not all momenta k can be excited into spin waves as long as $\xi_k > 1$ is fulfilled within a certain k-range, where the system is in the APT phase and the eigenfrequencies are pure imaginary. It is clear that such low-energy magnetization excitations are beyond the traditional Goldstone modes and can be realized by adjusting not only the Gilbert damping α but also the RKKY interactions J (cf the right column of figure 2). These full numerical simulations endorse the theoretical analysis as well as the experimental feasibility and relevance of the anti-$\mathcal{PT}$ symmetry breaking in SyAFM systems.

BIC controlled by DMI. Besides EP, BIC is a (standing) wave that remains perfectly confined without any radiation even though it falls within the continuum spectrum. BICs were originally proposed by von Neumann and Wigner for electronic systems [53] and have been observed experimentally in electromagnetic, acoustic, water and elastic waves [54–63]. The unique properties of BICs have led to numerous applications, including slow light, sensors, filters, and quantum memory. Here, we show that magnonic BICs can be generated by introducing the asymmetric DMI. This new kind of singularity maybe useful for SyAFM magnonics.

For systems hosting interfacial DMI, we incorporate in the theory the interaction

$$\mathcal{H}_{\rm DMI} = -D\mathbf{m}_n \cdot (\tilde{\nabla} \times \mathbf{m}_n), \tag{9}$$

where $\tilde{\nabla} = \hat{\mathbf{e}}_n \times \nabla$ with $\hat{\mathbf{e}}_n$ being the normal direction of DMI surfaces. For the one-dimensional SyAFM along the x-axis, the DMI contribute to the energy density with $H_n = -A\nabla^2 + K_z + J - \mathrm{i}D_n\nabla_x$. Note that $\hat{\mathbf{e}}_n$ is the normal direction of the upper or the lower surface of each FM sublayers, depending on where the DMI is dominantly generated. For the sake of discussion, we have assigned an effective value D_n to each magnetic layers. Two distinct magnonic BICs are then found in SyAFMs depending on whether they are anti-$\mathcal{PT}$ symmetric or not:

(a) Asymmetric SyAFMs with $D_1 = -D_{\bar{1}} = D$. The Hamiltonian $\mathcal{H}'$ has no $\mathcal{PT}$ or anti-$\mathcal{PT}$ symmetry. The dispersion relation is asymmetric giving rise to nonreciprocal spin waves. The intrinsic Gilbert damping is balanced by the introduced DMIs, resulting in $\omega_\pm = 0$, Friedrich–Wintgen (FW) [64] BICs (which occur in the vicinity of avoided crossing of two dispersion curves) appear as a pair, as shown in figure 3.

(b) Anti-$\mathcal{PT}$ symmetric SyAFMs with $D_1 = D_{\bar{1}} = D$. $\mathcal{H}'$ now still satisfies $\{\mathcal{H}', \hat{\mathcal{P}}\hat{\mathcal{T}}\} = 0$. In the APT phase, near the EPs, FW BICs emerge at $k_{\rm BIC} = (-D \pm \sqrt{D^2 - 4AK_z})/2A$ provided that the uniform

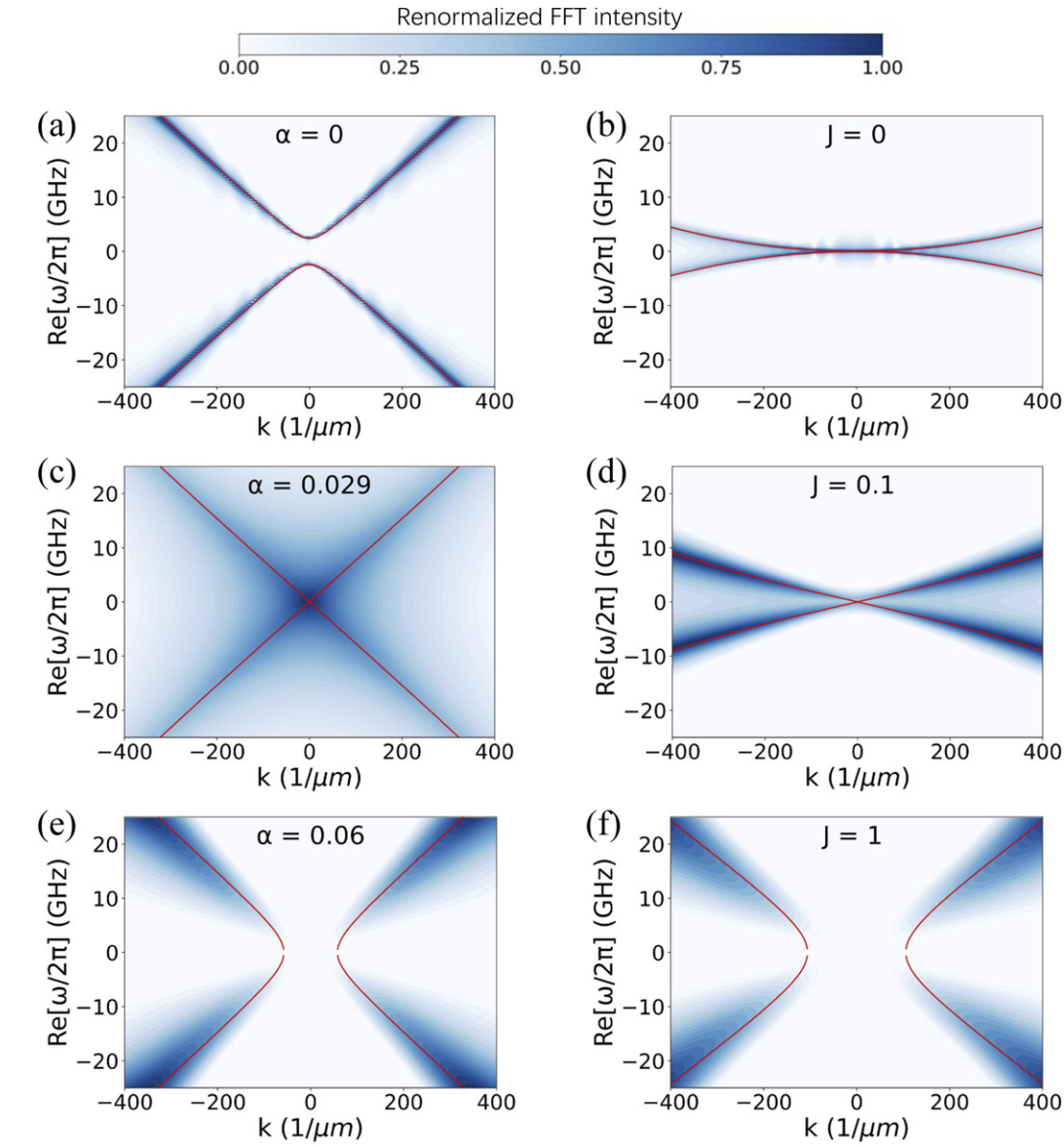

Figure 2. Density plot of the energy dispersion relation under different Gilbert damping α (left column) or RKKY interactions J (right column). The renormalized FFT intensities correspond to the micromagnetic simulation results. The analytical dispersions, as follow from equation (5) are shown by the red curves. (a), (c) and (e) are given with a fixed RKKY interaction $J = 1.2$ MJ m^{-3} (b), (d) and (f) are calculated with the same Gilbert damping constant $\alpha = 0.1$. In the simulations, we assumed for the exchange stiffness constant $A = 0.5$ pJ m^{-1} and for the magnetic anisotropy $K_z = 0.5$ kJ m^{-3}.

Néel-type AFM ordering is preserved in a narrow window beyond $D^2 \geqslant 4AK_z$ for the geometrically constrained system discussed here. Unlike the above BICs in asymmetric SyAFMs, these anti-$\mathcal{PT}$ symmetry-protected BICs are equator modes that stem from the maximal coherent superposition of magnetization excitations with 50–50 contributions from the upper and lower FM layers, as demonstrated by equation (6). They are further confirmed by the dynamic magnetic susceptibility ($\chi(\mathbf{k},\omega)$) or dynamics spin correlations ($\mathcal{S}_n(\mathbf{k},\omega) = \langle S_n^-(\mathbf{k})S_n^+(-\mathbf{k})\rangle_\omega$). Based on the linear response theory with $S_1^- = \delta m_1^x - \mathrm{i}\delta m_1^y$ and $S_1^+ = \delta m_1^x + \mathrm{i}\delta m_1^y$, one has

$$\chi(\mathbf{k},\omega) \propto \mathcal{S}_1(\mathbf{k},\omega) = \frac{\omega + H_n(1+\mathrm{i}\alpha)}{(\omega-\omega_+)(\omega-\omega_-)}. \tag{10}$$

As shown in figure 4, the imaginary part of the susceptibility $\Im\chi(\mathbf{k},\omega)$ diverges at the wavevector k_{BIC}, implying an infinite lifetime and a zero leakage rate of BICs. These unique hybridized modes are robust against the detuning parameters in the APT phase.

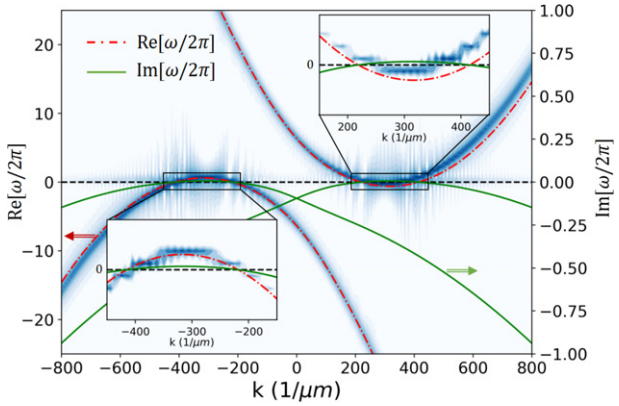

Figure 3. Energy dispersion relations of asymmetric SyAFMs with opposite DMIs. The density plot of FFT intensities are derived from the mircomagnetic simulations. The red and green curves correspond to the real and imaginary parts of eigenvalues with the DMI strength $D_1 = -D_{\bar{1}} = 0.7$ mJ m^{-2}. Other parameters are $A = 1.0$ pJ m^{-1}, $K_z = 35$ kJ m^{-3}, $J = 0.1$ MJ m^{-3} and Gilbert damping constant $\alpha = 0.01$. The regions with BICs are shown on an enlarged scale in the insets.

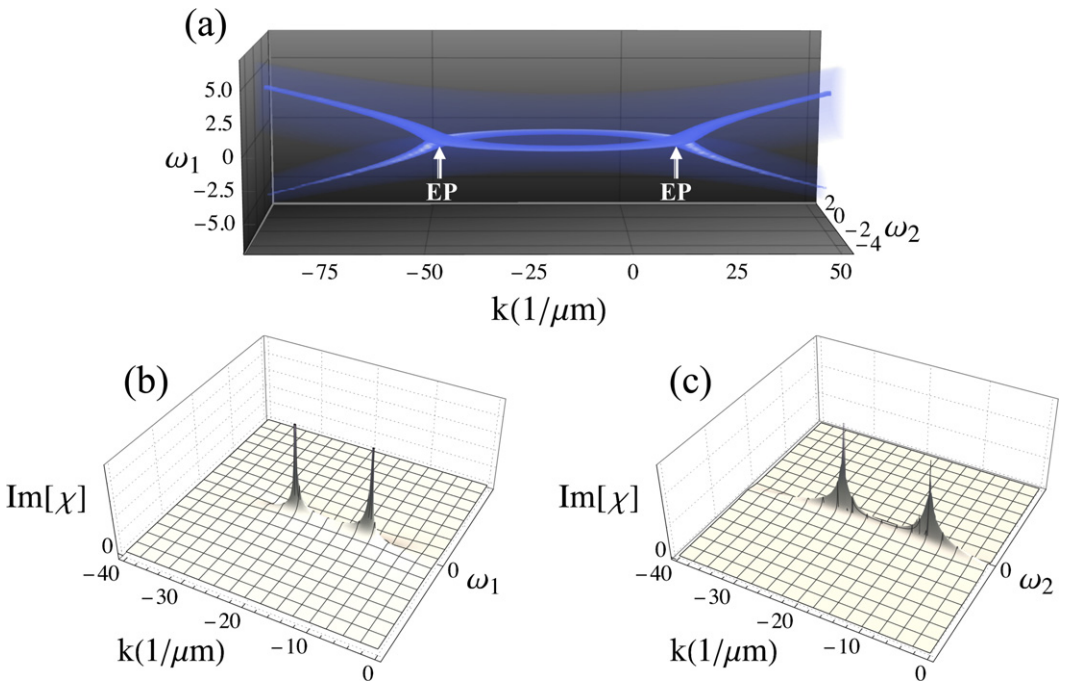

Figure 4. Dynamic magnetic susceptibility of SyAFMs with same DMIs. (a) Three-dimensional density plot of susceptibility $\chi(k, \omega)$ where the complex frequencies $\omega = \omega_1 + \mathrm{i}\omega_2$. The imaginary part of dynamic magnetic susceptibility $\Im\chi$ in the APT phase as functions of (b) ω_1, (c) ω_2 and the wave vector k. Other parameters are $A = 2.0$ pJ m^{-1}, $K_z = 0.5$ kJ m^{-3}, $J = 0.1005$ MJ m^{-3}, $\alpha = 0.2$, and $D = 68$ μJ m^{-2}. The BICs at $k_{\mathrm{BIC}} = -23.2$ μm^{-1} and -10.7 μm^{-1} are consistent with the analytical values.

3. Conclusions

As a typical dissipative system, the low-energy magnetization excitations in the balanced SyAFMs are shown to be eigenstates of the anti-$\mathcal{PT}$ symmetry operator for certain intrinsic parameters in the free energy density. Such parameters can be tuned by external probes or by material engineering, and the system can be driven to a phase with the low-energy modes are no longer eigenstates of the anti-$\mathcal{PT}$ operator. The phase transition between the symmetry-preserved and the symmetry-broken APT phase is accompanied with the emergence of a finite magnetization and bound states in the continuum with maximally coherent superposition for spin waves. These tunable singularities can be relevant to transport of magnons and imply numerous cross applications, such as magnon entanglement, slow spin waves, and magnonic quantum-information devices.

Acknowledgments

This work is supported by the National Natural Science Foundation of China (Nos. 12174164, 91963201, and 11834005), the German Research Foundation (SFB TRR 227), and the 111 Project under Grant No. B2006.

ORCID iDs

Chao-Wei Sui https://orcid.org/0000-0002-8075-3429
Xi-Guang Wang https://orcid.org/0000-0002-4154-8115
Jamal Berakdar https://orcid.org/0000-0001-8727-3981
Chenglong Jia https://orcid.org/0000-0003-2064-923X

References

[1] Jungwirth T, Marti X, Wadley P and Wunderlich J 2016 Antiferromagnetic spintronics *Nat. Nanotechnol.* **11** 231
[2] Duine R A, Lee K-J, Parkin S S P and Stiles M D 2018 Synthetic antiferromagnetic spintronics *Nat. Phys.* **14** 217
[3] Rezende S M, Azevedo A and Rodríguez-Suárez R L 2019 Introduction to antiferromagnetic magnons *J. Appl. Phys.* **126** 151101
[4] Chumak A V, Vasyuchka V I, Serga A A and Hillebrands B 2015 Magnon spintronics *Nat. Phys.* **11** 453
[5] Mahmoud A, Ciubotaru F, Vanderveken F, Chumak A V, Hamdioui S, Adelmann C and Cotofana S 2020 Introduction to spin wave computing *J. Appl. Phys.* **128** 161101
[6] Barman A *et al* 2021 The 2021 magnonics roadmap *J. Phys.: Condens. Matter* **33** 413001
[7] Prabhakar A and Stancil D D 2009 *Spin Waves:Theory and Applications* (Berlin: Springer)
[8] Lan J, Yu W, Wu R and Xiao J 2015 Spin-wave diode *Phys. Rev.* X **5** 041049
[9] Kajiwara Y *et al* 2010 Transmission of electrical signals by spin-wave interconversion in a magnetic insulator *Nature* **464** 262
[10] Parkin S S P, Hayashi M and Thomas L 2008 Magnetic domain-wall racetrack memory *Science* **320** 190
[11] Keffer F, Kaplan H and Yafet Y 1953 Spin waves in ferromagnetic and antiferromagnetic materials *Am. J. Phys.* **21** 250
[12] Cheng R, Daniels M W, Zhu J-G and Xiao D 2016 Antiferromagnetic spin wave field-effect transistor *Sci. Rep.* **6** 24223
[13] Wang X-g, Guo G-h and Berakdar J 2020 Steering magnonic dynamics and permeability at exceptional points in a parity-time symmetric waveguide *Nat. Commun.* **11** 5663
[14] Bender C M, Boettcher S and Meisinger P N 1999 $\mathcal{PT}$-symmetric quantum mechanics *J. Math. Phys.* **40** 2201
[15] Brandstetter M, Liertzer M, Deutsch C, Klang P, Schöberl J, Türeci H E, Strasser G, Unterrainer K and Rotter S 2014 Reversing the pump dependence of a laser at an exceptional point *Nat. Commun.* **5** 4034
[16] Bender C M, Berry M V and Mandilara A 2002 Generalized $\mathcal{PT}$ symmetry and real spectra *J. Phys. A: Math. Gen.* **35** L467
[17] Bender C M and Boettcher S 1998 Real spectra in non-Hermitian Hamiltonians having $\mathcal{PT}$ symmetry *Phys. Rev. Lett.* **80** 5243
[18] El-Ganainy R, Makris K G, Khajavikhan M, Musslimani Z H, Rotter S and Christodoulides D N 2018 Non-Hermitian physics and PT symmetry *Nat. Phys.* **14** 11
[19] Gardas B, Deffner S and Saxena A 2016 $\mathcal{PT}$-symmetric slowing down of decoherence *Phys. Rev.* A **94** 040101
[20] Guo A, Salamo G J, Morandotti R, Volatier-Ravat M, Aimez V, Siviloglou G A and Christodoulides D N 2009 Observation of PT-symmetry breaking in complex optical potentials *Phys. Rev. Lett.* **103** 093902
[21] Liu H, Sun D, Zhang C, Groesbeck M, Mclaughlin R and Vardeny Z V 2019 Observation of exceptional points in magnonic parity-time symmetry devices *Sci. Adv.* **5** eaax9144
[22] Lee J M, Kottos T and Shapiro B 2015 Macroscopic magnetic structures with balanced gain and loss *Phys. Rev.* B **91** 094416
[23] Katsantonis I, Droulias S, Soukoulis C M, Economou E N and Kafesaki M 2020 $\mathcal{PT}$-symmetric chiral metamaterials: asymmetric effects and $\mathcal{PT}$-phase control *Phys. Rev.* B **101** 214109
[24] Kepesidis K V, Milburn T J, Huber J, Makris K G, Rotter S and Rabl P 2016 $\mathcal{PT}$-symmetry breaking in the steady state of microscopic gain–loss systems *New J. Phys.* **18** 095003
[25] Monticone F, Valagiannopoulos C A and Alù A 2016 Parity-time symmetric nonlocal metasurfaces: all-angle negative refraction and volumetric imaging *Phys. Rev.* X **6** 041018
[26] Özdemir Ş K, Rotter S, Nori F and Yang L 2019 Parity-time symmetry and exceptional points in photonics *Nat. Mater.* **18** 783
[27] Peng B *et al* 2014 Parity-time-symmetric whispering-gallery microcavities *Nat. Phys.* **10** 394
[28] Regensburger A, Bersch C, Miri M-A, Onishchukov G, Christodoulides D N and Peschel U 2012 Parity-time synthetic photonic lattices *Nature* **488** 167
[29] Rüter C E, Makris K G, El-Ganainy R, Christodoulides D N, Segev M and Kip D 2010 Observation of parity-time symmetry in optics *Nat. Phys.* **6** 192
[30] Tserkovnyak Y 2020 Exceptional points in dissipatively coupled spin dynamics *Phys. Rev. Res.* **2** 013031
[31] Wang X-g, Guo G-h and Berakdar J 2021 Anti-enhanced sensitivity at magnetic high-order exceptional points and topological energy transfer in magnonic planar waveguides *Phys. Rev. Appl.* **15** 034050
[32] Li Y *et al* 2019 Anti-parity-time symmetry in diffusive systems *Science* **364** 170
[33] Antonosyan D A, Solntsev A S and Sukhorukov A A 2015 Parity-time anti-symmetric parametric amplifier *Opt. Lett.* **40** 4575
[34] Choi Y, Hahn C, Yoon J W and Song S H 2018 Observation of an anti-PT-symmetric exceptional point and energy-difference conserving dynamics in electrical circuit resonators *Nat. Commun.* **9** 2182
[35] Ge L and Türeci H E 2013 Antisymmetric PT-photonic structures with balanced positive and negative index materials *Phys. Rev.* A **88** 053810
[36] Konotop V V and Zezyulin D A 2018 Odd-time reversal PT symmetry induced by an anti-PT-symmetric medium *Phys. Rev. Lett.* **120** 123902
[37] Yang F, Liu Y C and You L 2017 Anti-PT symmetry in dissipatively coupled optical systems *Phys. Rev.* A **96** 053845
[38] Zhang F, Feng Y, Chen X, Ge L and Wan W 2020 Synthetic anti-PT symmetry in a single microcavity *Phys. Rev. Lett.* **124** 053901

[39] Zhao J, Liu Y, Wu L, Duan C K, Liu Y-x and Du J 2020 Observation of anti-PT symmetry phase transition in the magnon cavity magnon coupled system *Phys. Rev. Appl.* **13** 014053
[40] Peng P, Cao W, Shen C, Qu W, Wen J, Jiang L and Xiao Y 2016 Anti-parity-time symmetry with flying atoms *Nat. Phys.* **12** 1139
[41] Yang Q *et al* 2018 Ionic liquid gating control of RKKY interaction in FeCoB/Ru/FeCoB and $(Pt/Co)_2/Ru/(Co/Pt)_2$ multilayers *Nat. Commun.* **9** 991
[42] Wang X, Yang Q, Wang L, Zhou Z, Min T, Liu M and Sun N X 2018 E-field control of the RKKY interaction in FeCoB/Ru/FeCoB/PMN-PT (011) multiferroic heterostructures *Adv. Mater.* **30** 1803612
[43] Jia C, Wang F, Jiang C, Berakdar J and Xue D 2015 Electric tuning of magnetization dynamics and electric field-induced negative magnetic permeability in nanoscale composite multiferroics *Sci. Rep.* **5** 11111
[44] Jia C L, Wei T L, Jiang C J, Xue D S, Sukhov A and Berakdar J 2014 Mechanism of interfacial magnetoelectric coupling in composite multiferroics *Phys. Rev.* B **90** 054423
[45] Jiang C, Jia C, Wang F, Zhou C and Xue D 2018 Transformable ferroelectric control of dynamic magnetic permeability *Phys. Rev.* B **97** 060408
[46] Vaz C A F 2012 Electric field control of magnetism in multiferroic heterostructures *J. Phys.: Condens. Matter* **24** 333201
[47] Manipatruni S, Nikonov D E, Lin C-C, Prasad B, Huang Y-L, Damodaran A R, Chen Z, Ramesh R and Young I A 2018 Voltage control of unidirectional anisotropy in ferromagnet-multiferroic system *Sci. Adv.* **4** eaat4229
[48] Guo B and Ding S 2008 *Landau–Lifshitz Equations* (Singapore: World Scientific)
[49] Lan J, Yu W and Xiao J 2017 Antiferromagnetic domain wall as spin wave polarizer and retarder *Nat. Commun.* **8** 178
[50] Maamache M and Kheniche L 2020 Anti-$\mathcal{PT}$ symmetry for a non-Hermitian Hamiltonian *Prog. Theor. Exp. Phys.* **2020** 123A01
[51] Cheng R, Okamoto S and Xiao D 2016 Spin Nernst effect of magnons in collinear antiferromagnets *Phys. Rev. Lett.* **117** 217202
[52] Tveten E G, Müller T, Linder J and Brataas A 2016 Intrinsic magnetization of antiferromagnetic textures *Phys. Rev.* B **93** 104408
[53] Hsu C W, Zhen B, Stone A D, Joannopoulos J D and Soljačić M 2016 Bound states in the continuum *Nat. Rev. Mater.* **1** 16048
[54] Yang Y, Wang Y-P, Rao J W, Gui Y S, Yao B M, Lu W and Hu C-M 2020 Unconventional singularity in anti-parity-time symmetric cavity magnonics *Phys. Rev. Lett.* **125** 147202
[55] Wu J, Artoni M and La Rocca G C 2015 Parity-time-antisymmetric atomic lattices without gain *Phys. Rev.* A **91** 033811
[56] Azzam S I, Shalaev V M, Boltasseva A and Kildishev A V 2018 Formation of bound states in the continuum in hybrid plasmonic-photonic systems *Phys. Rev. Lett.* **121** 253901
[57] Bulgakov E N and Maksimov D N 2017 Topological bound states in the continuum in arrays of dielectric spheres *Phys. Rev. Lett.* **118** 267401
[58] Garmon S, Gianfreda M and Hatano N 2015 Bound states, scattering states, and resonant states in $\mathcal{PT}$-symmetric open quantum systems *Phys. Rev.* A **92** 022125
[59] Marinica D C, Borisov A G and Shabanov S V 2008 Bound states in the continuum in photonics *Phys. Rev. Lett.* **100** 183902
[60] Romano S, Zito G, Lara Yépez S N, Cabrini S, Penzo E, Coppola G, Rendina I and Mocellaark V 2019 Tuning the exponential sensitivity of a bound-state-in-continuum optical sensor *Opt. Express* **27** 18776
[61] Stillinger F H and Herrick D R 1975 Bound states in the continuum *Phys. Rev.* A **11** 446
[62] Xiao Y-X, Ma G, Zhang Z-Q and Chan C T 2017 Topological subspace-induced bound state in the continuum *Phys. Rev. Lett.* **118** 166803
[63] Zhen B, Hsu C W, Lu L, Stone A D and Soljačić M 2014 Topological nature of optical bound states in the continuum *Phys. Rev. Lett.* **113** 257401
[64] Friedrich H and Wintgen D 1985 Interfering resonances and bound states in the continuum *Phys. Rev.* A **32** 3231